

Selective adsorption and efficient removal of phosphate using lanthanum-modified mesoporous silica from aqueous solutions

Shaoqing Li, Yan Zhuang, Guizhen Li, Tianru Zou, Hongbin Wang, Wei Tan*, Min Yang*

School of Chemistry and Environment, Yunnan Minzu University, Kunming 650500, China, emails: 317366182@qq.com (W. Tan), 826677468@qq.com (M. Yang)

Received 16 June 2021; Accepted 16 September 2021

ABSTRACT

Lanthanum-modified mesoporous silica (MS-La) with a specific surface area of 386 m²/g was prepared using mesoporous silica and lanthanum(III) as raw materials by co-precipitation method. The composite adsorbent is ideal for the removal of solutions contaminated with phosphate, due to their chemical stability and a strong affinity with phosphate. MS-La could effectively removal of phosphate within the pH range of 3–6. The coexisting anions result manifested that MS-La with excellent selectivity to phosphate was determined by the hydrogen bonding mechanism in competitive anion solutions. The adsorption kinetics was well fitted with the pseudo-second-order kinetic equation, suggesting chemical adsorption. The Langmuir isothermal model could better describe the adsorption isotherm data and the maximum adsorption capacity of 27.98 mg/g. Furthermore, the main mechanism of phosphate adsorption was electrostatic attraction and ligand exchange. Its efficient adsorption capacity ensures a bright prospect for low-concentration phosphate removal.

Keywords: Mesoporous silica; Lanthanum; Phosphate; Adsorption

1. Introduction

Phosphorus (P) is an essential element of the structure of animals and plants, and it also maintains the dynamic balance of the ecological environment [1]. However, a large quantity of phosphate from untreated industrial wastewater and domestic sewage has been brought into rivers, lakes and oceans over the past decades. The excessive phosphate in the water induces eutrophication, which results in the exponential growth and reproduction of algae and plankton and reduced dissolved oxygen [2–4]. Therefore, it is extremely important to reduce the concentration of phosphate in sewage and improve the quality of sewage treatment and eliminate the eutrophication of water bodies.

Until now, the main methods of phosphate removal from water, including biological treatment [5], chemical precipitation [6] and adsorption [7], membrane separation [8] have been reported. However, the chemical precipitation is restricted due to the generation of large amounts of sludge and secondary pollution problems [9]. Biological treatment and membrane separation are displayed high efficiency, but it is costly [10,11]. However, adsorption shows more advantages due to no secondary pollution, fast adsorption speed, simple process, low cost and its wonderful performance in low-concentration phosphate removal [12,13]. Typically, adsorbents like bentonite, zeolite, and fly ash are used in phosphate removal. Whereas, its applications are limited because

* Corresponding authors.

of small surface area, difficult recovery and weak adaptability. Therefore, it is key to consider suitable adsorbents and reasonable morphology to remove selective phosphates from contaminated water. The main species of phosphate in water are H_2PO_4^- and HPO_4^{2-} as anions. The selectivity trend is completely depending on the Hofmeister series [14]. When the charge number of anions are equivalent, several materials are hydrophobic and they prefer lowly hydrated anions to highly hydrated ones [15,16]. Therefore, it is possible that the hydrogen bonding mechanism will drive out competing anions when removing monovalent and divalent phosphate species [11,17].

Mesoporous silica (MS) as a carrier has received considerable attention owing to its highly ordered and regular pore structure, a large number of silanol groups, high specific surface area and easy modification [18–20]. For example, the ligand embedded composite adsorbent based on mesoporous silica displayed rapid adsorption, significant selectivity and high adsorption capacity for phosphate removal in polluted wastewater [15]. Besides, a zirconia-doped mesoporous silica SBA-15 was studied. The high adsorption capacities for phosphate removal were attributed to Zr-OH combined with high surface sites [21]. Therefore, as a carrier, MS provides a great quantity of active sites for active materials, improving the adsorption efficiency of phosphate.

Previous studies have shown that lanthanum (La) used as an adsorbent in water treatment has a strong affinity with phosphate at low concentrations and the low solubility product of LaPO_4 ($\text{p}K_{\text{sp}} = 26.15$) [22–24]. Unfortunately, the lanthanum is not satisfying due to its poor mechanical strength [25,26]. To optimize the adsorption performance of La, a large number of studies focus on the preparation of composites like La-containing adsorbents. For example, La-porous zeolite composite (La-Z) was prepared, whose lanthanum oxide was successfully loaded on porous zeolite through the hydrothermal method. It can effectively adsorb phosphate in a pH range of 3.0–7.0 with its capacity of 17.2 mg/g [27]. Lanthanum-doped biochar (La-BC) was used by a chemical precipitation method. The maximum adsorption capacity of 46.37 mg/g was attributed to the doping of lanthanum [28]. Moreover, lanthanum-coated chitosan-montmorillonite composite (La-CS-MMT) was synthesized through hydrogen bonding and outer spherical complex formation for effective phosphate removal, and regeneration adsorption of the five cycles maintained at 70% [29]. Therefore, the introduction of lanthanum selective sites into the carrier can make great significance for the selectivity of specific targets, the use efficiency of La and its adsorption performance.

In this work, MS was used as a carrier to prepare lanthanum-modified mesoporous silica (MS-La) by the co-precipitation method for the removal of phosphate in water. The adsorbents were characterized by scanning electron microscopy (SEM), Brunauer–Emmett–Teller (BET), X-ray diffraction (XRD) and Fourier transform infrared spectrometer (FTIR). The adsorption behavior of phosphate from the aqueous solution was investigated, including the effect of contact time, adsorbent dose, pH value and coexisting anions for the removal of phosphate. At the same time, the adsorption kinetics, isotherm and thermodynamics

were studied, and the mechanism of phosphate adsorption was revealed.

2. Experiment

2.1. Chemicals and materials

Tetraethyl orthosilicate (TEOS) and cetyltrimethylammonium bromide (CTAB) were purchased by Sinopharm Chemical Reagent Co., Ltd., (Shanghai, China). Lanthanum nitrate hydrate [$\text{La}(\text{NO}_3)_3 \cdot 6\text{H}_2\text{O}$] was purchased from Guangfu Fine Chemical Research Institute (Tianjin, China). 0.2197g of KH_2PO_4 was dissolved in 1,000 mL of deionized water to prepare 50 mg/L phosphate deionized solution. All reagents were used as an analytical grade.

2.2. Preparation of the MS-La

MS-La in a previous report has been discussed that has an effective ability for the removal of fluorine [30]. MS was prepared by a sol-gel method and modified by a co-precipitation method to prepare an MS-La composite. To ensure the complete precipitation of La, NaHCO_3 was selected as the precipitant. The optimized preparation steps are as follows, firstly, 0.375 g of MS was added in 30 mL of deionized water. Secondly, $\text{La}(\text{CO}_3)_3 \cdot 6\text{H}_2\text{O}$ with La/Si molar ratio of 0.08 was added in MS solution and dissolved after stirring. Thirdly, NaHCO_3 solution with NaHCO_3/La molar ratio of 3.0 was slowly added, and the mixture was continuously stirred at room temperature for 10 h. Finally, the composites were washed with suction filtration and dried at 90°C overnight to prepare MS-La.

2.3. Sample characterization

The surface morphology of MS-La was observed by using scanning electron microscopy (SEM, Nova Nano-SEM-450, USA) combined with energy-dispersive X-ray spectroscopy (EDS) at an acceleration voltage of 20 kV. The crystal structure was determined using X-ray diffraction (XRD, D8AA25X, GER) under a $\text{Cu K}\alpha$ radiation in a 2 θ wavelength range of 10°–70°, with a 12°/min scanning speed and 0.01° step size. Brunauer–Emmett–Teller (BET, NOVA2000, USA) was used to determine the BET specific surface area, pore-volume, and pore size distribution of the adsorbent using N_2 as the adsorbate. The structure and composition were analyzed using a Fourier transform infrared spectrometer (FTIR, Nicolet iS10, USA). Samples were prepared using the potassium bromide tableting method with a resolution of 2 cm^{-1} and a scanning range of 400–4,000 cm^{-1} .

2.4. Phosphate adsorption experiment

The effect of contact time, adsorbent dose, pH value and coexisting anions on phosphate adsorption were performed successively. 40 mg of adsorbent was mixed with a 50 mL solution containing 10 mg/L phosphate solution in a conical flask at 150 rpm at room temperature for different contact time (0–300 min). The different adsorbents (10–100 mg) were mixed with 50 mL 10 mg/L phosphate solution for 3 h

to study the effect of adsorbents dosage. Similarly, to compare the effect of initial pH value on the adsorption of phosphate, 40 mg of adsorbent was added into 50 mL 10 mg/L phosphate solution at room temperature for 3 h with the pH range of 2–12 adjusted by HCl or NaOH solutions (1 M). To study the effect of coexisting anions, a certain concentration (0, 40, 80 and 150 mg/L) of HCO_3^- , Cl^- , SO_4^{2-} and NO_3^- were added to the solution respectively.

The kinetics of the adsorbent was studied as follows: 40 mg of adsorbent was added into 50 mL of the initial concentration of phosphate solution (20, 30, and 40 mg/L) at 150 rpm at room temperature. Adsorption isotherm experiments were performed at different temperatures (25°C, 35°C, and 45°C). In the experiment, 40 mg of adsorbent was added with an initial concentration of 5 to 80 mg/L phosphate at 150 rpm at room temperature for 3 h.

The phosphate concentrations were determined using the visible spectrophotometer (UNIC-7200, China) by molybdenum antimony anti-spectrophotometry (GB11893-89). The adsorption capacity at equilibrium Q_e (mg/g) and the percentage of removal $R(\%)$ are calculated by using Eqs. (1) and (2):

$$Q_e = \frac{(C_0 - C_e) \times V}{m \times 1000} \quad (1)$$

$$R(\%) = \frac{C_0 - C_e}{C_0} \times 100\% \quad (2)$$

where C_0 and C_e are the initial and equilibrium concentration of phosphate (mg/L), respectively; V is the volume of phosphate solution (mL) and m is the adsorbent dosage (mg).

3. Results and discussion

3.1. Characterization of MS-La

3.1.1. Scanning electron microscopy-energy-dispersive X-ray spectroscopy

The structural and morphological changes of MS and MS-La were characterized by SEM. As shown in Fig. 1a and b, MS synthesized by the sol-gel method with a clear spherical morphology, uniform dispersion, and uniform particle size, can provide La with a suitable surface-exposed position so that it can be evenly dispersed on the MS surface. Compared with MS, the image of the MS-La (shown in Fig. 1b) also has spherical morphology, but the particle has weak aggregates and the size of MS decreases after it combined with La. Lamellar structure could be found, which indicated that flaky $\text{La}_2(\text{CO}_3)_3$ were loaded and dispersed on the surface of MS. Besides, the

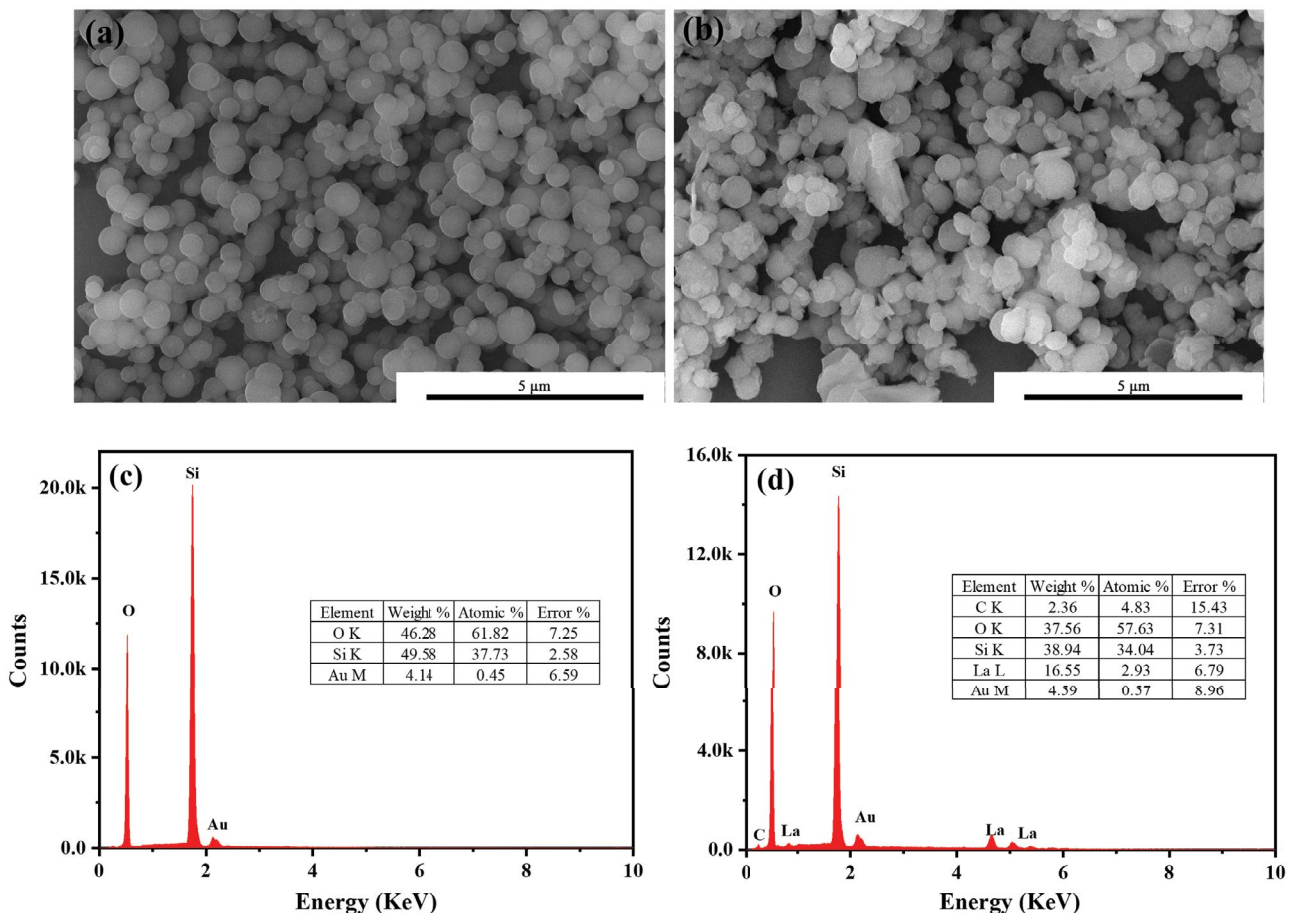


Fig. 1. SEM image of MS (a) and MS-La (b), EDS spectra of MS (c) and MS-La (d).

composition of MS and MS-La was tested by EDS and the result is shown in Fig. 1c and d. The main compositions on the surface of MS were mainly O and Si, whose average weight percentages were 46.28% and 49.58%, respectively. The chemical compositions and average weight percentage of MS-La were C (2.36%), O (37.56), Si (38.94%) and La (16.55%), respectively. Si/La (wt%/wt%) was 2.35, which was close to the calculating one (2.52), indicating the high effective combination efficiency. The sample also contained a certain quantity of Au, which may be come from the pretreatment during the test.

3.1.2. Brunauer–Emmett–Teller

The porous structure of MS before and after modification with La was confirmed by BET measurement. The N_2 adsorption–desorption isotherms and Barrett–Joyner–Halenda distributions curves of MS and MS-La are shown in Fig. 2a–d. From Fig. 2a we can see the adsorption amount increases sharply when relative pressure (P/P_0) changed from 0.2 to 0.3, which shows a typical type IV isotherm, suggesting typical mesoporous structural features [31]. On the other side, seen from the pore size distribution (Fig. 2b), the pore size of MS is mainly concentrated at about 3.14 nm. Compared with MS, the N_2 adsorption–desorption isotherms curves of MS-La (Fig. 2b)

shows similar the type IV isotherm, which can be explained homogeneous growth of La in the MS [32]. The pore size of MS-La (Fig. 2d) was concentrated in the mesoporous range. Experimental data of specific surface area (S_{BET}), pore size and pore volume are summarized in Table 1. As shown in Table 1, S_{BET} decreased from 1,363.51 to 386.23 m^2/g , and the pore size also decreased from 3.14 to 2.05 nm after modification. Similarly, the pore volumes dropped from 0.227 to 0.162 cm^3/g . The presence of La led to a reduction in S_{BET} total pore volume and pore size. Meanwhile, these main changes in MS as carriers confirmed the successful loading of La into MS-La, which obtained more active sites and improved the adsorption efficiency of phosphate.

3.1.3. X-ray diffraction

The XRD pattern of MS and MS-La are shown in Fig. 3. In the pattern of MS, a broad peak centered at around $2\theta = 24^\circ$, which was assigned to the amorphous mesoporous SiO_2 (JCPDS No. 29-0085) [26]. By the load of La, one could observe the appearance of three peaks at 2θ values of 18.3° , 20.8° and 27.8° (indicated by a star), which correspond to the (020), (004) and (220) crystal facets of $La_2(CO_3)_3$. However, the diffraction peak became weaker, it may be that part of the pores of MS were blocked and the crystallinity is weakened.

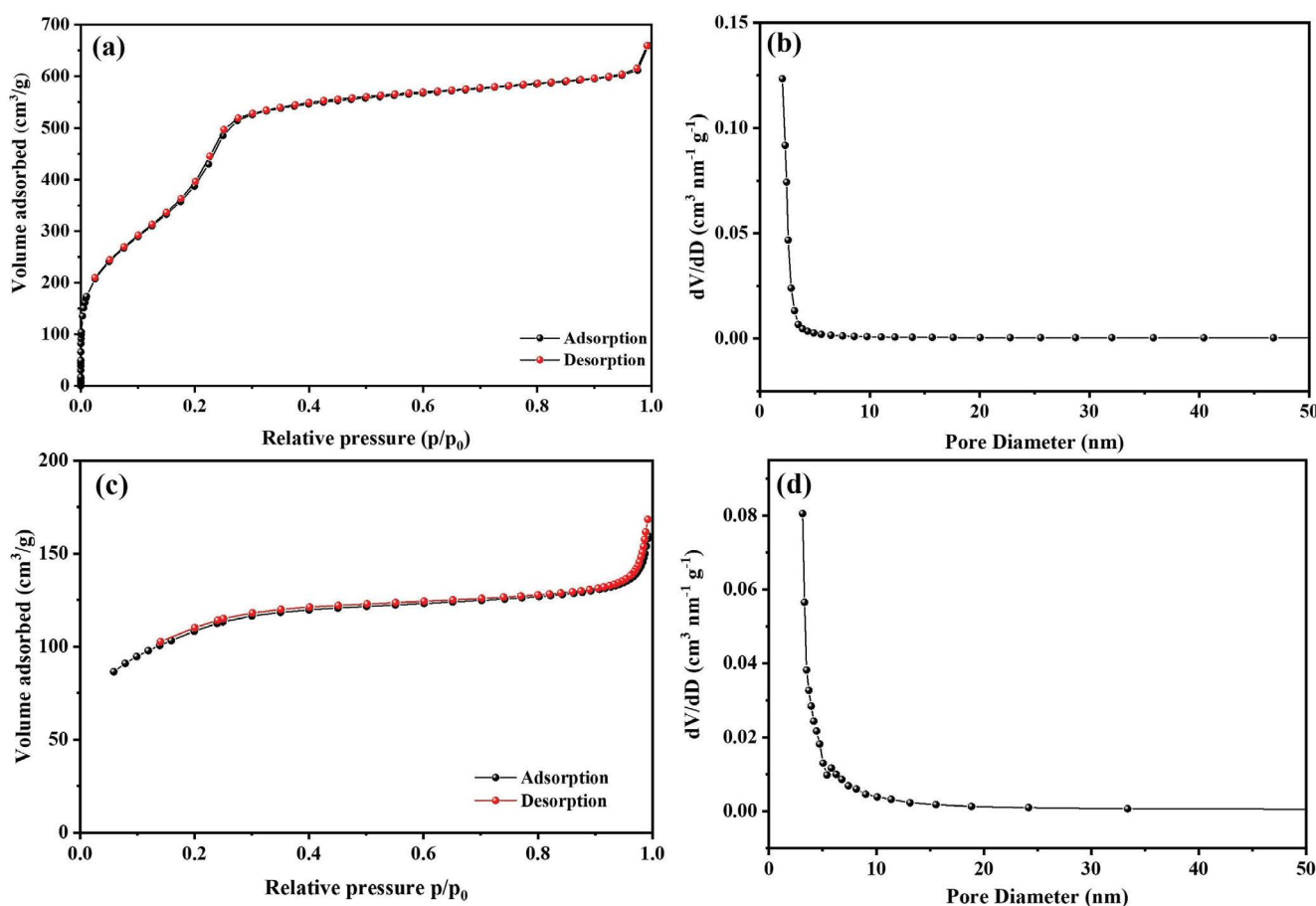


Fig. 2. N_2 adsorption–desorption isotherms and Barrett–Joyner–Halenda distributions of MS (a,b) and MS-La (c,d).

Table 1
Surface area, pore size and pore volume of MS and MS-La

Sample	Surface area (S_{BET}) (m^2/g)	Pore size (nm)	Pore volume (cm^3/g)
MS	1,363.51	3.14	0.227
MS-La	386.23	2.05	0.162

3.1.4. Fourier transform infrared spectrometer

The FTIR spectra of MS and MS-La before and after phosphate adsorption are shown in Fig. 4. All the samples showed that a broad peak at about 3438 cm^{-1} in the hydroxyl region was assigned to the O–H stretching vibration mode of surface-adsorbed water molecules [33], and the stretching vibration of a small amount of uncondensed silanol group (Si–OH) [34]. The peak at 1645 cm^{-1} corresponded to C = O stretching vibration. The peaks at near 1090 , 800 and 476 cm^{-1} were attributed to the asymmetric, symmetric and bending stretching vibration of Si–O–Si, respectively [35]. The FTIR spectra of MS-La before adsorption of phosphate, a small peak observed at 1480 cm^{-1} was due to the bending vibration mode of La–OH. After phosphate, the MS-La showed a new peak of 613 cm^{-1} corresponding to the O–P–O bending vibration [36]. A peak at 1050 cm^{-1} was assigned to the asymmetric P–O stretching vibration, which coincided with the stretching vibration of asymmetrical Si–O–Si, resulting in a broader peak [37].

3.2. Optimization of the adsorption conditions

3.2.1. Effect of contact time

The contact time of MS-La in the phosphate adsorption is presented in Fig. 5a. It shows that the phosphate adsorption increases rapidly in the first 60 min, and then the adsorption increased slowly until it reached the adsorption equilibrium at 180 min. This may attribute to the presence of more adsorption sites at the beginning

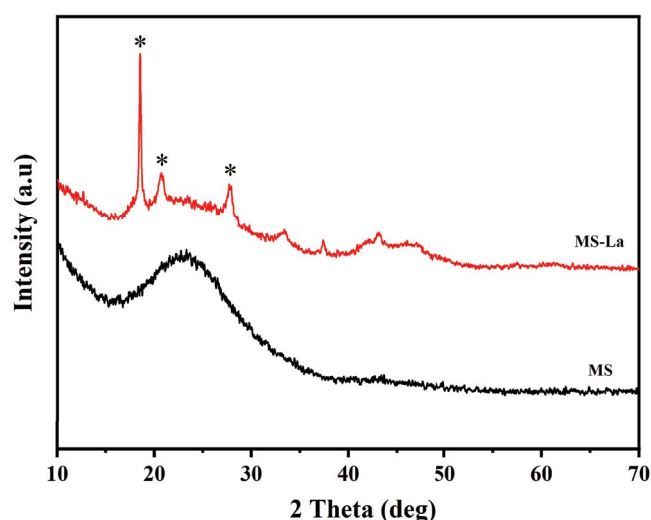


Fig. 3. XRD patterns of MS and MS-La.

of the adsorbents, and a higher driving force provided by the gradient of phosphate concentration in the aqueous solution [38]. With the increase of time, a subsequent decrease in the adsorption rate due to the adsorption sites were gradually occupied by phosphate.

3.2.2. Effect of adsorbents dosage

To assess the optimal conditions for adsorbent dosage on phosphate adsorption, the effects of MS-La dosages (10–100 mg) are given in Fig. 5b. With the increase of adsorbents dosage from 10 to 50 mg, the removal efficiency of phosphate increased from 25.85% to 97.35%. The removal efficiency increased little or none with the increase in the number of adsorbents (>50 mg). It was a possible reason that removal efficiency reached the stage of removal limit, further increase of the dosage had insignificant effects. Thus, the final experiment confirmed 50 mg as the optimal amount of adsorbents.

3.2.3. Effect of initial pH

Typically, the initial pH is regarded as a key factor during the adsorption process. It is known that phosphate have multiple forms of existence (Fig. S1), including H_3PO_4 , H_2PO_4^- , HPO_4^{2-} and PO_4^{3-} , which are highly relative to the dissociation equilibrium constant of phosphate ($\text{p}K_1 = 2.1$, $\text{p}K_2 = 7.2$, $\text{p}K_3 = 12.7$) [39]. The effect of initial pH on

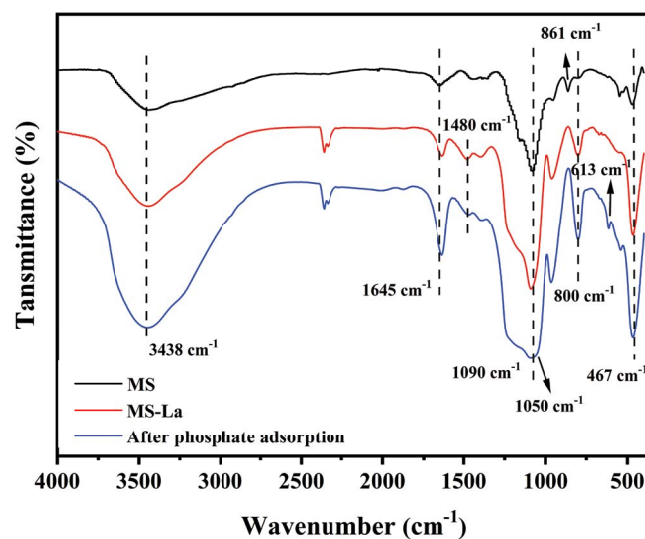


Fig. 4. FTIR spectra of MS, MS-La before and after phosphate adsorption.

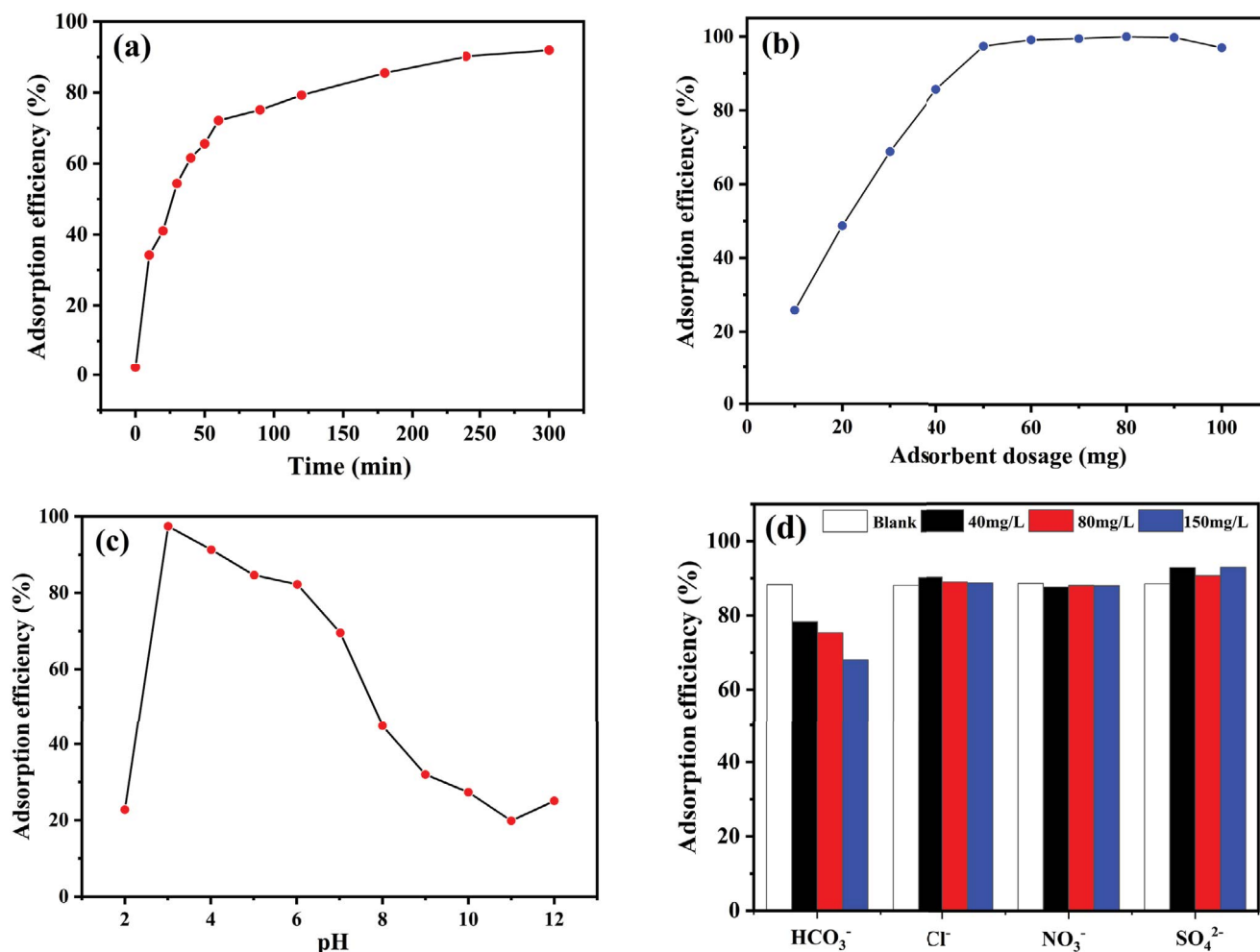


Fig. 5. Effect of contact time (a), adsorbent dosage (b), initial pH (c) and coexisting anions (d) for phosphate adsorption.

phosphate removal by MS-La is presented in Fig. 5c. The removal efficiency of adsorbent exhibited an upward trend when the pH of the solution was between 2.0 and 3.0. The removal efficiency increased to 97.4% at pH of 3.0, so the optimal pH for phosphate removal was 3. When pH from 3.0 to 6.0, the phosphate adsorption efficiency dropped gradually, but maintained this relatively high level, above 80%. While the adsorption efficiency decreased from 82.2% to 19.8% between pH 6.0 to 12.0. This trend was probably due to the fact that, when $\text{pH} \leq 2.0$, the main form of phosphate species in the solution was H_3PO_4 which was weakly combined with adsorbents of positive charge [40]. With the gradual increase of pH, the presence of dominant phosphate species was H_2PO_4^- at pH 3.0–6.0. Due to the surface charge effect, the negatively charged H_2PO_4^- combined with the adsorbents was beneficial to the occurrence of adsorption. Furthermore, the existence of phosphate species was transformed into HPO_4^{2-} when $\text{pH} > 6$. It was a possible reason that a large number of hydroxide ions did not favor the protonation of $\text{La}_2(\text{CO}_3)_3$, and it will strongly compete with the phosphate on the active sites. The results caused that more negative charges to accumulate on the surface of the adsorbents reduced the adsorption efficiency [25].

3.2.4. Effect of coexisting anions

Many coexisting anions of different concentrations have a large difference for removal phosphates. The effects of single coexisting anions, including Cl^- , NO_3^- , HCO_3^- and SO_4^{2-} , on phosphate adsorption, are shown in Fig. 5d. When introducing 40 mg/L HCO_3^- , the adsorption efficiency reduced by 9%. However, the presence of Cl^- , NO_3^- and SO_4^{2-} exerted negligible effects on phosphate adsorption. After the addition of coexisting anions with concentrations of 150 mg/L, the presence of other anions also did not affect the adsorption process, which suggested that the adsorbents possessed a high selectivity for phosphate. The high selectivity is mainly determined by the hydrogen bonding mechanism. Highly basic anions possess lone pairs of electrons with high electron density, so that prefer to form hydrogen bonds with protonated $\text{La}_2(\text{CO}_3)_3$. For example, the alkalinity of HPO_4^{2-} is greater than that of SO_4^{2-} , so the protonated adsorbent is more likely to bind to HPO_4^{2-} rather than other anions. Therefore, the selectivity of the composite adsorbent is higher than other competing anions [15,41,42]. Besides, the presence of HCO_3^- reduced adsorption efficiency by 20%. On the one hand, the addition

of HCO_3^- increased the pH in the solution, which affected the distribution of phosphate species. On the other hand, compared with the other three anions, HCO_3^- might have a higher affinity for the adsorbents to strongly compete with HPO_4^{2-} in the solution, and thus it significantly deteriorated the absorption of phosphate by the adsorbents [33].

3.3. Adsorption kinetics

To better evaluate the adsorption efficiency and understand the adsorption mechanism, the adsorption kinetic of MS-La for phosphate adsorption was investigated. The pseudo-first-order and pseudo-second-order models were used to study the phosphate adsorption behavior. Eqs. (3) and (4) used are as follows:

Pseudo-first-order:

$$Q_t = Q_e (1 - e^{-k_1 t}) \quad (3)$$

Pseudo-second-order:

$$Q_t = \frac{K_L Q_e^2 t}{1 + k_2 Q_e t} \quad (4)$$

where Q_e and Q_t are the adsorption capacity at equilibrium (mg/g) and over a given period time (mg/g), respectively; t is the adsorption time (min); k_1 (min^{-1}) and k_2 (g/mg min) are the pseudo-first-order and pseudo-second-order adsorption rate constant, respectively.

The kinetic data were tested by using the pseudo-first-order and pseudo-second-order models. The results are illustrated in Fig. S2a–c, and the kinetic parameters and coefficients are summarized in Table 2. The results demonstrated that the pseudo-second-order model better described the adsorption behavior of MS-La and obtained higher coefficient of determination ($R^2 > 0.98$) than the pseudo-first-order model, suggesting that the chemical adsorption occurred on phosphate adsorption.

3.4. Adsorption isotherm

The equilibrium adsorption isotherm is used to explain the interaction between the adsorbates and the adsorbents [43]. Through different temperatures (25°C, 35°C and 45°C), the adsorption capacity was studied under the initial concentration of phosphate at 5–80 mg/L. The Langmuir adsorption model and Freundlich adsorption model were used to study the adsorption performance of the adsorbents. Eqs. (5) and (6) used are as follows:

Langmuir adsorption isotherm:

$$Q_e = \frac{Q_{\max} K_L C_e}{1 + K_L C_e} \quad (5)$$

Freundlich adsorption isotherm:

$$Q_e = K_F C_e^{1/n} \quad (6)$$

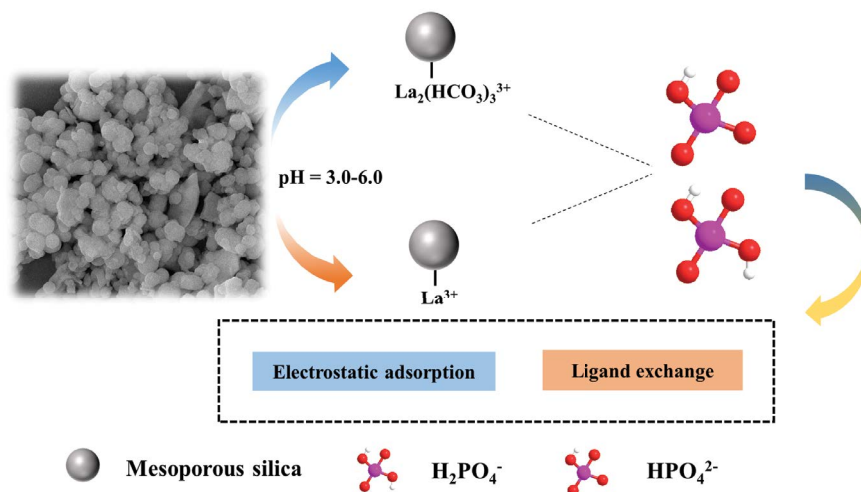


Fig. 6. Adsorption mechanism of MS-La removed phosphate.

Table 2
Kinetic parameters for phosphate adsorption by MS-La

C_0 (mg/L)	$Q_{e,\text{exp}}$ (mg/g)	Pseudo-first-order kinetic			Pseudo-second-order kinetic		
		Q_e (mg/g)	k_1 (min^{-1})	R^2	Q_e (mg/g)	k_2 (g/mg min)	R^2
20	22.99	21.44	0.034	0.9681	24.34	0.0015	0.9908
30	24.09	22.53	0.051	0.9532	24.91	0.0030	0.9819
40	28.30	27.31	0.032	0.9695	30.79	0.0018	0.9835

where Q_{\max} and Q_e are the maximum adsorption capacity (mg/g) and the adsorption capacity at equilibrium (mg/g), respectively; C_e is the equilibrium concentration of phosphate (mg/L); K_L is the Langmuir constants (L/mg); K_f is the Freundlich constant (mg/g); n is an empirical constant related to temperature.

According to Langmuir and Freundlich models, the adsorption isotherms of MS-La composites for phosphate adsorption are studied in Fig. S3a and b. The calculated values of the Freundlich and Langmuir model parameters are shown in Table 3. Compared with Freundlich isothermal model, the adsorption data could be better fitted by the Langmuir adsorption model with much larger coefficient of determination ($R^2 > 0.98$), indicating that the adsorption process occurs on the surface of MS-La via homogeneous monolayer adsorption [44]. In Table 3, the maximum adsorption capacity decided from the Langmuir model was 27.98 mg/L at 25°C. The value of Q_{\max} did not change significantly as an increase in temperature, suggesting that the adsorption between phosphate and MS-La was less effected by temperature. Additionally, several inorganic adsorbents have been used for the adsorption of phosphate, as summarized in Table 4. It is clearly seen that the present MS-La provides an obviously improvement on the adsorption capacity with respect to the previously reported adsorbents.

3.5. Adsorption thermodynamics

The energy changes, thermodynamic parameters were used to investigate the adsorption process, including Gibbs free energy (ΔG°), enthalpy change (ΔH°) and entropy change (ΔS°). The thermodynamic parameters are calculated by Eqs. (7)–(9):

$$K_d = 1000 \frac{Q_e}{C_e} \quad (7)$$

$$\Delta G^\circ = -RT \ln K_d \quad (8)$$

$$\ln K_d = \frac{\Delta S^\circ}{R} - \frac{\Delta H^\circ}{RT} \quad (9)$$

where R is the gas constant (8.314 J/K mol); T is the adsorption temperature (K); K_d is adsorption equilibrium constant; Q_e is the adsorption capacity at equilibrium (mg/g); C_e is the equilibrium concentration of phosphate.

At different temperatures (25°C, 35°C and 45°C), the values of ΔS° and ΔH° were determined by plotting

$\ln K_d$ vs. $1/T$, and the value of ΔG° was calculated. The thermodynamic parameters of MS-La for phosphate adsorption are shown in Table 5. At all temperatures, the negative value of ΔG° in the adsorption process from -15.33 to -16.51 kJ/mol with a rise in temperature from 25°C to 45°C, suggesting that the increase of spontaneity at higher temperatures and the physical adsorption mechanism existed in the adsorption process [38]. Hence, the adsorption mechanisms occurred between MS-La and phosphate were both physical adsorption and chemical adsorption. The positive value of ΔH° proved endothermic nature during the adsorption process. This result was consistent with the adsorption isotherm (Fig. S3 and Table 3). Moreover, the positive value of ΔS° demonstrated that phosphate had a good affinity for the adsorbent and the randomness increased at the solid-liquid interface during the adsorption of phosphate on MS-La [51].

3.6. Possible adsorption mechanisms

The functional groups on the surface of materials might result in protonation at different pH [52]. Similarly, $\text{La}_2(\text{CO}_3)_3$ on the surface of MS-La might be protonated under acidic or alkaline conditions. $\text{La}_2(\text{CO}_3)_3$ started to transform into $\text{La}_2(\text{HCO}_3)_3^{3+}$ in the pH value of 2–3 according to Eq. (10), and the adsorption efficiency of phosphate showed a rapid upward trend. The main species of phosphate in solution changed from H_3PO_4 to H_2PO_4^- . However, the adsorption efficiency of phosphate presented lower due to the presence of H_3PO_4 . As the initial pH increased from 3.0 to 6.0, $\text{La}_2(\text{HCO}_3)_3^{3+}$ and La^{3+} [Eq. (11)] became the main species on the surface of the material. The surface positive charge of adsorbents combined with phosphates

Table 4
Comparison of adsorption capacity of some inorganic adsorbents for phosphate adsorption

Adsorbents	Adsorption capacity (mg/g)	Reference
La-doped activated carbon	22.86	[45]
Fe-Si-La	27.8	[46]
MCM-41 silica with rice husk	21.01	[47]
La(III) modified zeolite	24.6	[48]
FMS-0.1La	42.76	[31]
La-alginate bentonite	6.74	[49]
La-alginate talc	16.4	[50]
MS-La	27.98	This work

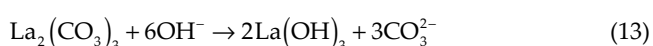
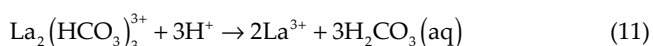
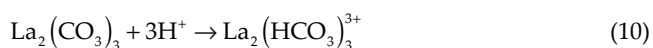
Table 3
Adsorption isotherm parameters for phosphate adsorption by MS-La

Temperature (°C)	Langmuir model			Freundlich model		
	Q_{\max} (mg/g)	K_L (L/mg)	R^2	K_f (mg/g)	n	R^2
25	27.98	1.573	0.9907	15.03	6.097	0.9022
35	26.82	2.655	0.9806	15.94	6.757	0.8074
45	27.49	2.162	0.9945	15.94	6.920	0.8944

Table 5
Thermodynamic parameters for phosphate adsorption by MS-La

ΔH° (kJ/mol)	ΔS° (J/mol K)	ΔG° (kJ/mol)		
		25°C	35°C	45°C
2.24	58.90	-15.33	-15.88	-16.51

of different species (H_2PO_4^- and HPO_4^{2-}). Thus, electrostatic interaction and ligand exchanges might be the important mechanisms of phosphate removal. With the continual increase of pH, $\text{La}_2(\text{HCO}_3)_3^{3+}$ was converted to $\text{La}_2(\text{CO}_3)_3$ and $\text{La}(\text{OH})_3$, according to Eqs. (12) and (13). $\text{La}_2(\text{HCO}_3)_3^{3+}$ on the surface of the materials were consumed in large quantities, which brought about weakening electrostatic adsorption. At this point of time, the surface of the MS-La existed a large number of hydroxyl groups and hydroxide, which can ligand exchange with phosphate [53].



Besides, The FTIR spectra after phosphate adsorption is shown in Fig. 3b. Some new peaks, such as 613 cm^{-1} and $1,050\text{ cm}^{-1}$ could be observed. Specifically, a peak at 613 cm^{-1} corresponded to O–P–O bending vibration. Another band at $1,050\text{ cm}^{-1}$ was assigned to the asymmetric stretching vibration of P–O. It was proved that the LaPO_4 precipitation exists. In short, this result was consistent with the adsorption mechanism of phosphates by other lanthanum-based adsorbents [54,55].

4. Conclusion

In summary, based on the high phosphate affinity of lanthanum and an ordered mesoporous structure of mesoporous silica were synthesized and used as the adsorbent for the removal of phosphate. The adsorption capacity of phosphate depended on the solution pH value and demonstrated effective removal of phosphate in the pH range of 3–6. The adsorption process was fitted well with the pseudo-second-order kinetic model and the Langmuir model. Besides, the adsorption thermodynamics were also determined, which demonstrated that the phosphate adsorption was a spontaneous and endothermic process. The efficient adsorption capacity can be attributed to electrostatic adsorption and ligand exchange on the MS-La surface. Therefore, the adsorbent could be used as an effective approach for removing phosphate in practical waters.

Acknowledgements

The authors gratefully thank the financial support of the Science Research Fund Projects of Department of

Education of Yunnan Province (No. 2020J0329, 2020J0327) and the 2019 Undergraduate Innovation and Entrepreneurship Training Projects of Yunnan Province.

References

- [1] L. Wang, J. Wang, W. Yan, C. He, Y. Shi, MgFe_2O_4 -biochar based lanthanum alginate beads for advanced phosphate removal, *Chem. Eng. J.*, 387 (2020) 123305, doi: 10.1016/j.cej.2019.123305.
- [2] T.K. Das, Q. Scott, A.N. Bezbaruah, Montmorillonite-iron crosslinked alginate beads for aqueous phosphate removal, *Chemosphere*, 281 (2021) 130837, doi: 10.1016/j.chemosphere.2021.130837.
- [3] I.W. Almanassra, V. Kochkodan, G. McKay, M.A. Atieh, T. Al-Ansari, Review of phosphate removal from water by carbonaceous sorbents, *J. Environ. Manage.*, 287 (2021) 112245, doi: 10.1016/j.jenvman.2021.112245.
- [4] Md. Rabiul Awual, S.A. El-Safty, A. Jyo, Removal of trace arsenic(V) and phosphate from water by a highly selective ligand exchange adsorbent, *J. Environ. Sci.*, 23 (2011) 1947–1954.
- [5] G. Guo, D. Wu, T. Hao, H.R. Mackey, L. Wei, G. Chen, Denitrifying sulfur conversion-associated EBPR: the effect of pH on anaerobic metabolism and performance, *Water Res.*, 123 (2017) 687–695.
- [6] H. Huang, J. Liu, L. Ding, Recovery of phosphate and ammonia nitrogen from the anaerobic digestion supernatant of activated sludge by chemical precipitation, *J. Cleaner Prod.*, 102 (2015) 437–446.
- [7] A. Shahat, H.M.A. Hassan, H.M.E. Azzazy, M. Hosni, Md. Rabiul Awual, Novel nano-conjugate materials for effective arsenic(V) and phosphate capturing in aqueous media, *Chem. Eng. J.*, 331 (2018) 54–63.
- [8] R. Liu, Y. Sui, X. Wang, Metal-organic framework-based ultrafiltration membrane separation with capacitive-type for enhanced phosphate removal, *Chem. Eng. J.*, 371 (2019) 903–913.
- [9] K. Zhou, B. Wu, L. Su, W. Xin, X. Chai, Enhanced phosphate removal using nanostructured hydrated ferric-zirconium binary oxide confined in a polymeric anion exchanger, *Chem. Eng. J.*, 345 (2018) 640–647.
- [10] Md. Rabiul Awual, M.A. Shenashen, T. Yaita, H. Shiwaku, A. Jyo, Efficient arsenic(V) removal from water by ligand exchange fibrous adsorbent, *Water Res.*, 46 (2012) 5541–5550.
- [11] Md. Rabiul Awual, A. Jyo, S.A. El-Safty, M. Tamada, N. Seko, A weak-base fibrous anion exchanger effective for rapid phosphate removal from water, *J. Hazard. Mater.*, 188 (2011) 164–171.
- [12] K. Lamont, E. Pensini, P. Daguppati, R. Rudra, J. van de Vegte, J. Levangie, Natural reusable calcium-rich adsorbent for the removal of phosphorus from water: proof of concept of a circular economy, *Can. J. Civ. Eng.*, 46 (2019) 458–461.
- [13] X. Jing, Y. Jiang, Y. Wang, E. Liu, R. Cheng, J. Dai, X. Dai, C. Li, Y. Yan, Phosphate removal using free-standing functionalized mesoporous silica films with excellent recyclability, *Microporous Mesoporous Mater.*, 296 (2020) 109953, doi: 10.1016/j.micromeso.2019.109953.
- [14] Md. Rabiul Awual, A. Jyo, Rapid column-mode removal of arsenate from water by crosslinked poly (allylamine) resin, *Water Res.*, 43 (2009) 1229–1236.
- [15] Md. Rabiul Awual, Efficient phosphate removal from water for controlling eutrophication using novel composite adsorbent, *J. Cleaner Prod.*, 228 (2019) 1311–1319.
- [16] Md. Rabiul Awual, A. Jyo, Assessing of phosphorus removal by polymeric anion exchangers, *Desalination*, 281 (2011) 111–117.
- [17] Md. Rabiul Awual, A. Jyo, T. Ihara, N. Seko, M. Tamada, K.T. Lim, Enhanced trace phosphate removal from water by zirconium (IV) loaded fibrous adsorbent, *Water Res.*, 45 (2011) 4592–4600.
- [18] A. Shahat, H.M.A. Hassan, M.F. El-Shahat, O. El Shahawy, Md. Rabiul Awual, Visual nickel(II) ions treatment in petroleum samples using a mesoporous composite adsorbent, *Chem. Eng. J.*, 334 (2018) 957–967.

- [19] M. Prokopowicz, K. Czarnobaj, A. Szewczyk, W. Sawicki, Preparation and in vitro characterisation of bioactive mesoporous silica microparticles for drug delivery applications, *Mater. Sci. Eng. C*, 60 (2016) 7–18.
- [20] B. Han, N. Chen, D. Deng, S. Deng, I. Djerdj, Y. Wang, Enhancing phosphate removal from water by using ordered mesoporous silica loaded with samarium oxide, *Anal. Methods*, 7 (2015) 10052–10060.
- [21] Y. Tang, E. Zong, H. Wan, Z. Xu, S. Zheng, D. Zhu, Zirconia functionalized SBA-15 as effective adsorbent for phosphate removal, *Microporous Mesoporous Mater.*, 155 (2012) 192–200.
- [22] X. Li, Y. Kuang, J. Chen, D. Wu, Competitive adsorption of phosphate and dissolved organic carbon on lanthanum-modified zeolite, *J. Colloid Interface Sci.*, 574 (2020) 197–206.
- [23] F.H. Firsching, S.N. Brune, Solubility products of the trivalent rare-earth phosphates, *J. Chem. Eng. Data*, 36 (1991) 93–95.
- [24] Y. Zhi, C. Zhang, R. Hjorth, A. Baun, O.W. Duckworth, D.F. Call, D.R.U. Knappe, J.L. Jones, K. Grieger, Emerging lanthanum(III)-containing materials for phosphate removal from water: a review towards future developments, *Environ. Int.*, 145 (2020) 106115, doi: 10.1016/j.envint.2020.106115.
- [25] H. Qiu, C. Liang, J. Yu, Q. Zhang, M. Song, F. Chen, Preferable phosphate sequestration by nano-La(III) (hydr) oxides modified wheat straw with excellent properties in regeneration, *Chem. Eng. J.*, 315 (2017) 345–354.
- [26] X. Jing, Y. Wang, L. Chen, Y. Wang, X. Yang, Y. Jiang, Y. Yan, Free-standing large-mesoporous silica films decorated with lanthanum as new adsorbents for efficient removal of phosphate, *J. Mol. Liq.*, 296 (2019) 111815, doi: 10.1016/j.molliq.2019.111815.
- [27] Y. He, H. Lin, Y. Dong, L. Wang, Preferable adsorption of phosphate using lanthanum-incorporated porous zeolite: characteristics and mechanism, *Appl. Surf. Sci.*, 426 (2017) 995–1004.
- [28] Z. Wang, D. Shen, F. Shen, T. Li, Phosphate adsorption on lanthanum loaded biochar, *Chemosphere*, 150 (2016) 1–7.
- [29] H.T. Banu, P. Karthikeyan, S. Meenakshi, Lanthanum(III) encapsulated chitosan-montmorillonite composite for the adsorptive removal of phosphate ions from aqueous solution, *Int. J. Biol. Macromol.*, 112 (2018) 284–293.
- [30] R. Wang, L. Luo, Y.J. Yang, S. Li, V. Jegatheesan, H.B. Wang, M. Yang, Preparation and characterization of mesoporous silica (MS) supporting lanthanum carbonate (MS-La) for the defluorination of aqueous solutions, *Desal. Water Treat.*, 96 (2017) 112–119.
- [31] W. Huang, X. Yu, J. Tang, Y. Zhu, Y. Zhang, D. Li, Enhanced adsorption of phosphate by flower-like mesoporous silica spheres loaded with lanthanum, *Microporous Mesoporous Mater.*, 217 (2015) 225–232.
- [32] C. Li, Y. Zhang, X. Wang, X. Yin, N. Luo, A. Khayambashi, Y. Wei, The synthesis and characterization of hydrous cerium oxide nanoparticles loaded on porous silica micro-sphere as novel and efficient adsorbents to remove phosphate radicals from water, *Microporous Mesoporous Mater.*, 279 (2019) 73–81.
- [33] P. Koilraj, K. Sasaki, Selective removal of phosphate using La-porous carbon composites from aqueous solutions: batch and column studies, *Chem. Eng. J.*, 317 (2017) 1059–1068.
- [34] J.X. He, M.Y. Cui, Y.Y. Zheng, W.H. Tang, B.Y. Chen, K. Tsukamoto, C.R. Li, Self-assembly of modified silica nanospheres at the liquid/liquid interface, *Mater. Lett.*, 64 (2010) 463–465.
- [35] L. Chen, Y. Li, Y. Sun, Y. Chen, J. Qian, La(OH)₃ loaded magnetic mesoporous nanospheres with highly efficient phosphate removal properties and superior pH stability, *Chem. Eng. J.*, 360 (2019) 342–348.
- [36] J. Xie, Z. Wang, S. Lu, D. Wu, Z. Zhang, H. Kong, Removal and recovery of phosphate from water by lanthanum hydroxide materials, *Chem. Eng. J.*, 254 (2014) 163–170.
- [37] I.T. Lucas, A.S. McLeod, J.S. Syzdek, D.S. Middlemiss, C.P. Grey, D.N. Basov, R. Kostecki, IR near-field spectroscopy and imaging of single Li₂FePO₄ microcrystals, *Nano Lett.*, 15 (2015) 1–7.
- [38] X. Liu, L. Zhang, Removal of phosphate anions using the modified chitosan beads: adsorption kinetic, isotherm and mechanism studies, *Powder Technol.*, 277 (2015) 112–119.
- [39] R. Saad, S. Hamoudi, K. Belkacemi, Adsorption of phosphate and nitrate anions on ammonium-functionalized mesoporous silicas, *J. Porous Mater.*, 15 (2008) 315–323.
- [40] M.Y. Can, E. Yildiz, Phosphate removal from water by fly ash: factorial experimental design, *J. Hazard. Mater.*, 135 (2006) 165–170.
- [41] Arsenate removal from water by a weak-base anion exchange fibrous adsorbent, *Water Res.*, 42 (2008) 689–696.
- [42] Md. Rabiul Awual, T. Yaita, S. Suzuki, H. Shiwaku, Ultimate selenium(IV) monitoring and removal from water using a new class of organic ligand based composite adsorbent, *J. Hazard. Mater.*, 291 (2015) 111–119.
- [43] X. Jia, X. He, K. Han, Y. Ba, X. Zhao, Q. Zhang, La₂O₃-modified MCM-41 for efficient phosphate removal synthesized using natural diatomite as precursor, *Water Sci. Technol.*, 79 (2019) 1878–1886.
- [44] J. Lin, Y. Zhan, H. Wang, M. Chu, C. Wang, Y. He, X. Wang, Effect of calcium ion on phosphate adsorption onto hydrous zirconium oxide, *Chem. Eng. J.*, 309 (2017) 118–129.
- [45] L. Zhang, J. Liu, L. Wan, Q. Zhou, X. Wang, Batch and fixed-bed column performance of phosphate adsorption by lanthanum-doped activated carbon fiber, *Water Air Soil Pollut.*, 223 (2012) 5893–5902.
- [46] L. Lai, Q. Xie, L. Chi, W. Gu, D. Wu, Adsorption of phosphate from water by easily separable Fe₃O₄@SiO₂ core/shell magnetic nanoparticles functionalized with hydrous lanthanum oxide, *J. Colloid Interface Sci.*, 465 (2016) 76–82.
- [47] M.K. Seliem, S. Komarneni, M.R. Abu Khadra, Phosphate removal from solution by composite of MCM-41 silica with rice husk: kinetic and equilibrium studies, *Microporous Mesoporous Mater.*, 224 (2016) 51–57.
- [48] P. Ning, H.-J. Bart, B. Li, X. Lu, Y. Zhang, Phosphate removal from wastewater by model-La(III) zeolite adsorbents, *J. Environ. Sci.*, 20 (2008) 670–674.
- [49] I.A. Kumar, N. Viswanathan, Fabrication of metal ions cross-linked alginate assisted biocomposite beads for selective phosphate removal, *J. Environ. Chem. Eng.*, 5 (2017) 1438–1446.
- [50] B. Wang, W. Zhang, L. Li, W. Guo, J. Xing, H. Wang, X. Hu, W. Lyu, R. Chen, J. Song, L. Chen, Z. Hong, Novel talc encapsulated lanthanum alginate hydrogel for efficient phosphate adsorption and fixation, *Chemosphere*, 256 (2020) 127124, doi: 10.1016/j.chemosphere.2020.127124.
- [51] W. Huang, J. Chen, F. He, J. Tang, D. Li, Y. Zhu, Y. Zhang, Effective phosphate adsorption by Zr/Al-pillared montmorillonite: insight into equilibrium, kinetics and thermodynamics, *Appl. Clay Sci.*, 104 (2015) 252–260.
- [52] R.M. Ali, H.A. Hamad, M.M. Hussein, G.F. Malash, Potential of using green adsorbent of heavy metal removal from aqueous solutions: adsorption kinetics, isotherm, thermodynamic, mechanism and economic analysis, *Ecol. Eng.*, 91 (2016) 317–332.
- [53] H. Hao, Y. Wang, B. Shi, NaLa(CO₃)₂ hybridized with Fe₃O₄ for efficient phosphate removal: synthesis and adsorption mechanistic study, *Water Res.*, 155 (2019) 1–11.
- [54] Y. Wu, X. Li, Q. Yang, D. Wang, Q. Xu, F. Yao, F. Chen, Z. Tao, X. Huang, Hydrated lanthanum oxide-modified diatomite as highly efficient adsorbent for low-concentration phosphate removal from secondary effluents, *J. Environ. Manage.*, 231 (2019) 370–379.
- [55] Y. Park, C. Gorman, E. Ford, Lanthanum carbonate nanofibers for phosphorus removal from water, *J. Mater. Sci.*, 55 (2020) 1–13, doi: 10.1007/s10853-019-04324-8.

Supplementary information

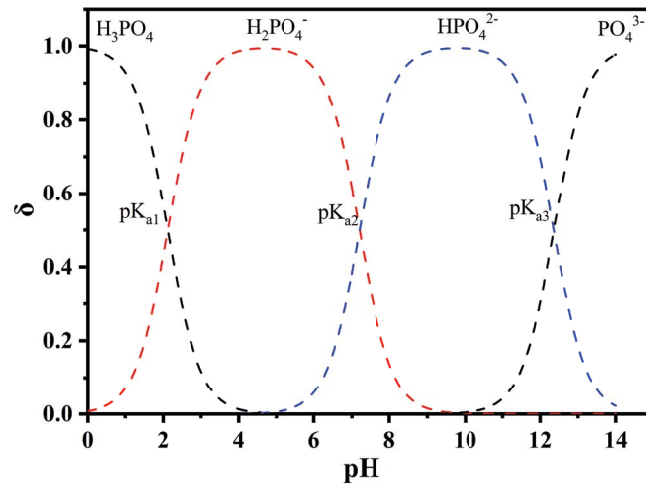


Fig. S1. The fraction of phosphate species at different pH.

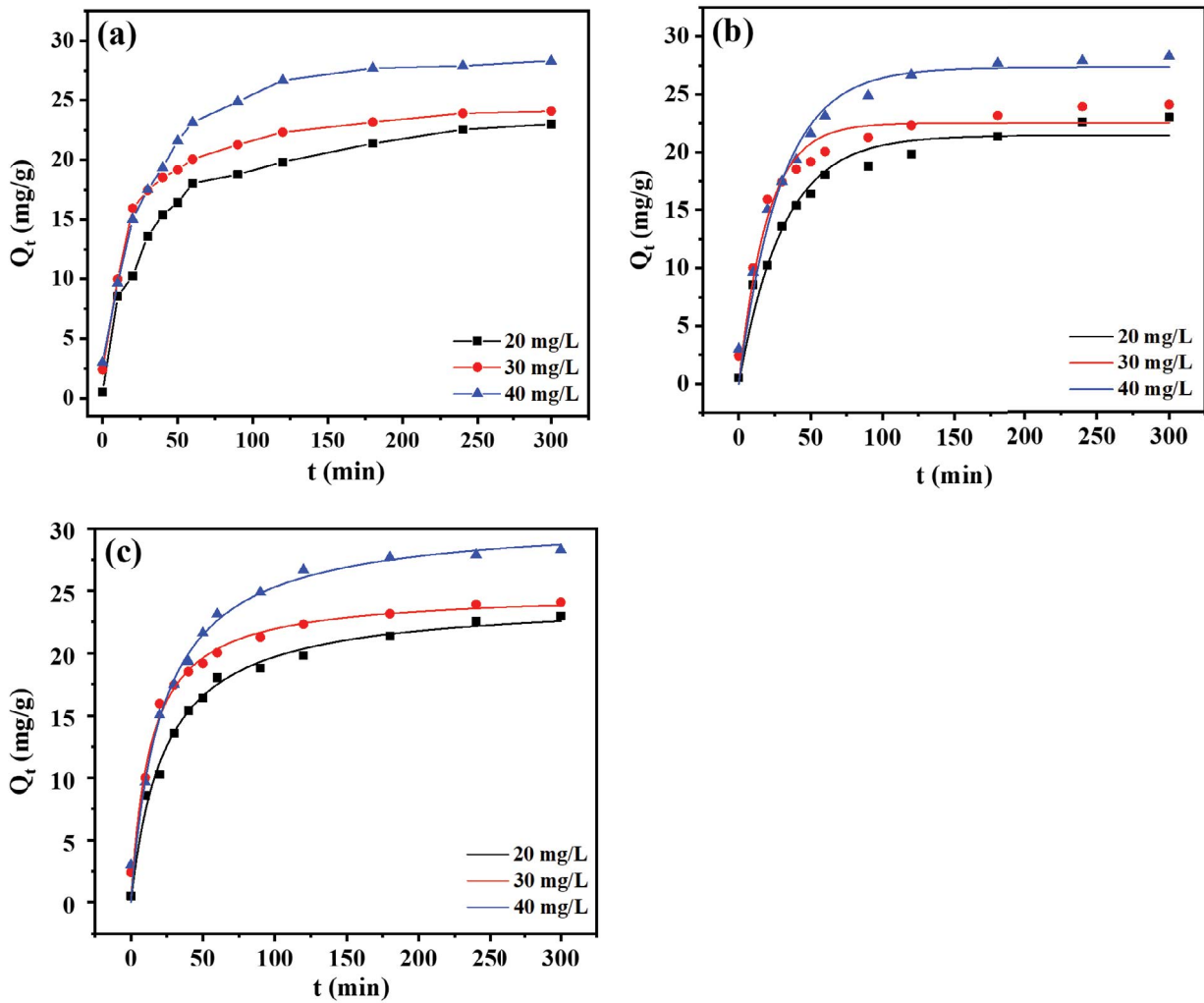


Fig. S2. Time-dependent kinetics (a), pseudo-first-order (b) and pseudo-second-order (c) for phosphate adsorption by MS-La.

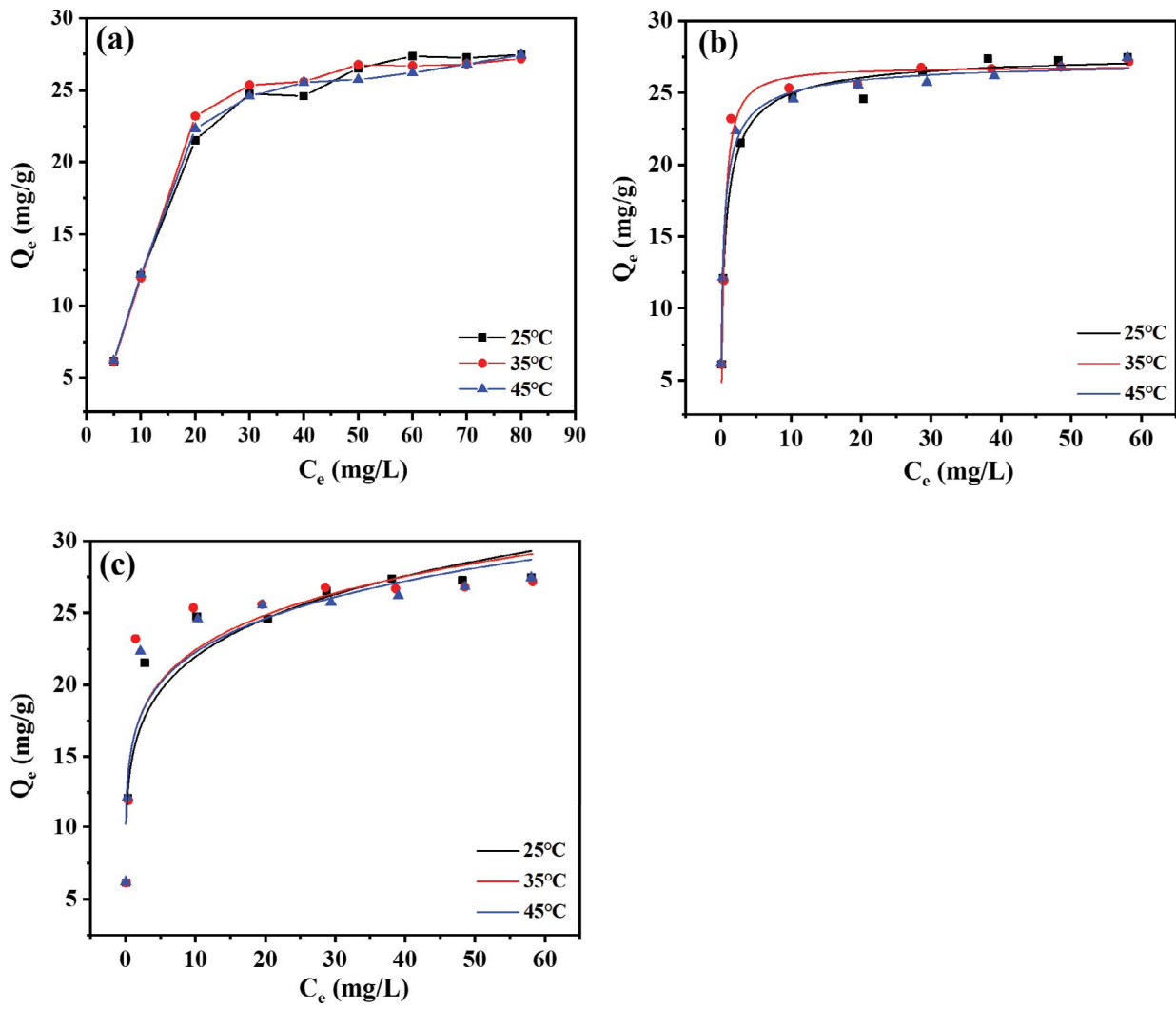


Fig. S3. Adsorption isotherm (a), the Langmuir model (b) and Freundlich model (c) for phosphate adsorption by MS-La.